



## Environmental mineralization of caffeine micro-pollutant by Fe-MFI zeolites

Julius Motuzas, Martin Drobek, Dana Martens, Cyril Vallicari, Anne Julbe,  
João Diniz da Costa

### ► To cite this version:

Julius Motuzas, Martin Drobek, Dana Martens, Cyril Vallicari, Anne Julbe, et al.. Environmental mineralization of caffeine micro-pollutant by Fe-MFI zeolites. Environmental Science and Pollution Research, 2018, 25 (4), pp.3628 - 3635. 10.1007/s11356-017-0530-0 . hal-01723029

**HAL Id: hal-01723029**

**<https://hal.umontpellier.fr/hal-01723029>**

Submitted on 18 Nov 2022

**HAL** is a multi-disciplinary open access archive for the deposit and dissemination of scientific research documents, whether they are published or not. The documents may come from teaching and research institutions in France or abroad, or from public or private research centers.

L'archive ouverte pluridisciplinaire **HAL**, est destinée au dépôt et à la diffusion de documents scientifiques de niveau recherche, publiés ou non, émanant des établissements d'enseignement et de recherche français ou étrangers, des laboratoires publics ou privés.

[Click here to view linked References](#)

# Environmental mineralization of caffeine micro-pollutant by Fe-MFI zeolites

*Julius Motuzas<sup>a\*</sup>, Martin Drobek<sup>b</sup>, Dana L. Martens<sup>a</sup>, Cyril Vallicar<sup>b</sup>, Anne Julbe<sup>b</sup> and  
João C. Diniz da Costa<sup>a</sup>*

<sup>a</sup>The University of Queensland, FIM<sup>2</sup>Lab – Functional Interfacial Materials and  
Membranes, School of Chemical Engineering, St. Lucia, Qld 4072, Australia.

<sup>b</sup>Institut Européen des Membranes, UMR 5635-CNRS-ENSCM-UM, Université de  
Montpellier, cc 047, Place Eugène Bataillon, 34095 Montpellier – Cedex 5, France.

\* Corresponding author: J. Motuzas; Tel: +61 7 3365 8835; Fax: +61 7 3365 4199;

Email: [j.motuzas@uq.edu.au](mailto:j.motuzas@uq.edu.au)

**Key words:** Fe-MFI; zeolite; caffeine; micro-pollutant; mineralization; Fenton reaction.

## Abstract

Environmentally emerging micro-pollutant, caffeine, was mineralized (i.e full degradation) by the isomorphic incorporation of Fe into silicalite-1 (MFI structure zeolite) through a microwave synthesis method. The Fe incorporation conferred mesopore formation that facilitated caffeine access and transport to the MFI zeolite structure. Increasing the Fe content favored the formation of Fe(O)<sub>4</sub> sites within the MFI structure. The catalytic activity for the degradation of caffeine increased as a function of Fe(O)<sub>4</sub> sites via a Fenton-like

heterogeneous reaction, otherwise not attainable using Fe-free pure MFI zeolites. Caffeine degradation reached 96% (TOC based) for zeolites containing 2.33% of Fe.

## 1. Introduction

Caffeine is rapidly becoming a contemporary anthropogenic pollutant in natural waters. It has been found in lakes in Switzerland (Buerge et al., 2003) and in the sea coast of Oregon (Rodriguez del Rey et al., 2012) in the USA. Caffeine pollution may be caused by effluents from our current lifestyle, related to drinking coffee and many energy drinks containing caffeine. Although the caffeine toxicity is of little concern for humans under moderate conditions, a similar generalization for aquatic organisms cannot be made since they are continuously exposed over a lifetime (Bruton et al., 2010). Hence, it is imperative to avoid future detrimental environmental impacts if caffeine continues to accumulate in natural waters. Caffeine can be degraded biochemically by *Pseudomonas* bacteria (Gummadi et al., 2009), by photolysis (Bruton et al., 2010), or by using chemical processes such as ozonation (Rosal et al., 2009). Advanced oxidation processes (AOPs) are also attractive in tackling caffeine degradation, particularly due to the simplicity of coupling catalysts and oxidants in a single unit operation. One of the most promising AOPs is the heterogeneous Fenton reaction using iron oxide catalyst and hydrogen peroxide ( $\text{H}_2\text{O}_2$ ) oxidant (Klamerth et al., 2012, Zeng et al., 2015). In this reaction, the active sites ( $\equiv\text{Fe}^{2+}$ ) react with  $\text{H}_2\text{O}_2$  and generate  $\cdot\text{OH}$  radical, a powerful oxidant extensively used in the degradation of organic compounds in wastewaters by AOPs processes (Zubir et al., 2015, Mijangos et al., 2006). The Fenton reaction approach was recently investigated for caffeine degradation using bio-based combined iron oxide photo

catalysts (Franzoso et al., 2017) and persulfated activated iron catalysts (S. Rodríguez et al., 2017).

Zeolites are efficient materials for separation (Rangnekar et al., 2015), adsorption (Hoffmann et al., 1997) and catalysis (Vermeiren and Gilson, 2009 and Li et al., 2014) applications, though they are generally used as adsorbents in water and wastewater treatment (Kragovi et al., 2013, An, 2013 and Wingenfelder et al., 2005). They can be prepared and used as either purely microporous or hierarchical micro/mesoporous materials (Pérez-Ramírez et al., 2008) . The latter form decreases diffusion restrictions and is widely applied in sorption (Meng et al., 2011) and catalysis (Christensen et al., 2003). A large variety of functionalities, such as acid-base or redox centers, can be introduced in zeolites (Moliner, 2012). Heteroatoms, such as Fe, can be incorporated in zeolites through various methods such as cationic exchange, impregnation, or chemical vapor deposition of metal precursors after zeolite crystallization (post-synthesis treatment). Another strategy, called “one pot”, consists in the direct insertion of heteroatoms during zeolite formation (Bordiga et al., 1996, Giordano et al., 2002); and is an attractive option for lowering the manufacturing costs and ensuring uniform dispersion of heteroatoms in either framework or extra-framework positions.

*In-situ* hydrothermal synthesis methods have been used to provide isomorphic incorporation of Fe into MFI zeolite structure, although reports to date have limited the Si/Fe molar ratio to 100 (1 at%Fe) (Kritchayanon et al., 2006; [Taniguchi et al., 2016](#)). Further Fe incorporation can be carried out by post-synthesis methods, but they mostly yield extra-framework iron oxide species (Maxwell et al., 2003; [Anizelli et al., 2016](#)). The isomorphic incorporation of iron species into zeolites differs from conventional

immobilization of iron-based particles (e.g. Fe, Fe<sub>2</sub>O<sub>3</sub> or Fe<sub>3</sub>O<sub>4</sub>) on substrates such as graphene oxides (Zubir et al., 2014), silica shells (Liu et al, 2014), carbon aerogels (Wang et al., 2013) or clays (Gao et al., 2015). The main advantage of inserting transition elements in zeolites by direct synthesis is related to the possibility of achieving a high dispersion of the metal in the zeolitic structure.

Herein, we show the production of higher Fe content Fe-MFI zeolites confers enhanced catalytic performance for the mineralization of caffeine as compared to traditional pure MFI zeolites. The as-synthesized Fe-MFI zeolites were tested for the catalytic caffeine removal from synthetic wastewaters under the conditions of the Fenton-like heterogeneous reaction. The catalytic testing was accompanied by the characterization of Fe-MFI zeolites. Of particular interest, the catalytic results are correlated to the role played by Fe–O sites in the mesoporous zeolite structure, in order to provided new insights into the improved catalytic efficiency of Fe-MFI zeolites.

## 2. Experimental

### 2.1. Materials Synthesis

The zeolite synthesis solutions were prepared by mixing TEOS (98%, Aldrich), ultrapure water (18.2 MΩ), tetrapropyl ammonium hydroxide (TPAOH, 20 wt% aqueous solution, Sigma) and iron (III) acetylacetonate (Fe(acac)<sub>3</sub>, 99.9%, Alfa Aesar). The sol molar concentration was set at (x/2) Fe<sub>2</sub>O<sub>3</sub> :100 SiO<sub>2</sub> : 40 TPAOH : 1950 H<sub>2</sub>O : 400 C<sub>2</sub>H<sub>5</sub>OH where x is the required atomic concentration of Fe in the MFI zeolite. Subsequently, the sols were aged under stirring for 24 h at 25 °C. The aged sols were placed into autoclaves in a commercial laboratory microwave oven (Milestone ETHOS 1600). The hydrothermal

1  
2  
3  
4 87 treatment was conducted as one pot synthesis. Initially, the closed autoclaves were  
5  
6 88 irradiated for 90 min at 80 °C with a MW power of 250 W. Subsequently, the autoclaves  
7  
8  
9 89 were heated to 180 °C and left for 60 min under MW irradiation of 400 W. Finally, the  
10  
11 90 autoclaves were cooled down to 50 °C before opening. The formed solid products were  
12  
13 91 separated by centrifugation at 9500 rpm (JOUAN B4i) and washed twice with distilled  
14  
15 92 water. A centrifugation step followed after each wash. The washed solids were dried for  
16  
17 93 4 h at 155 °C prior to calcination. The dried materials were then calcined in air at 550 °C  
18  
19 94 for 8 h with heating and cooling rates of 5 °C min<sup>-1</sup>.  
20  
21  
22

23 95 Characterization. A PANalytical X'Pert Pro X-ray diffractometer operating at 40 mA and  
24  
25 96 40 kV was used for measurement of X-ray diffraction patterns. PANalytical X'pert Pro  
26  
27 97 software was used to determine the crystal phase and calculate the lattice constants.  
28  
29 98 Morphological features of the samples were observed on a Hitachi S-4800 field emission  
30  
31 99 scanning electron microscope (FESEM), and a JEOL JMS-2010 high resolution  
32  
33 100 transmission electron microscope (HR-TEM). The elemental composition of samples was  
34  
35 101 assessed using a JEOL Model JSM-7001F SEM system equipped for energy-dispersive  
36  
37 102 X-ray spectroscopy (EDS). X-ray spectra were collected with a JEOL Minicup EDS  
38  
39 103 detector (Model EX-64175JMH), with a 133 eV resolution, 10 mm<sup>2</sup> effective area, polymer  
40  
41 104 ultrathin window (UTW) and using JEOL Analysis Station JED-2300 Series (v. 3.84)  
42  
43 105 software. Microanalysis acquisition conditions were 20 keV at 10 mm working distance.  
44  
45  
46  
47  
48  
49  
50

51 106 The descriptors (x%Fe-MFI) for the samples are based on the Fe content detected in  
52  
53 107 the solid ascertained by EDS, where x represents the atomic percentage of Fe in (Si+Fe)  
54  
55 108 mixture within the zeolite sample (i.e. x=0.34 (0.34%Fe-MFI)). A Renishaw inVia confocal  
56  
57 109 Raman Microscope Spectrometer operated with UV laser line (325 nm) was employed  
58  
59  
60  
61  
62  
63  
64  
65

for Raman measurements. The Raman spectra were deconvoluted using Origin 8.5 software. Nitrogen sorption measurements were performed on a Micromeritics TriStar 3020 analyzer after degassing at 300 °C for 24 h under vacuum on a VacPrep061 degassing system. Specific surface area values were calculated by Brunauer-Emmett-Teller (BET) model, from adsorption data in the 0.05–0.20 relative pressure range ( $p/p_o$ ). Pore diameters were determined via the density functional theory (DFT) modeling of the entire adsorption branch ( $p/p_o = 0.0005$ – $0.95$ ) using a cylindrical pore model on metal oxide surface with a regularization factor of 0.40. The minimum size modeled by DFT ( $12\text{\AA}$ ) was limited by the lower limit value of the relative pressure ( $p/p_o \sim 5 \times 10^{-4}$ ).

## 2.2. Catalysis experiments

The catalytic activity of materials was tested using  $0.33\text{ g L}^{-1}$  zeolite and a commercial  $\text{Fe}_3\text{O}_4$  (98%, Sigma-Aldrich), deionized water at pH of 3 (adjusted by HCl, 36%wt, Chem-supply Pty Ltd) and 22 mM hydrogen peroxide ( $\text{H}_2\text{O}_2$ , 30%, Chem-supply Pty Ltd.). The caffeine concentration was varied from 10 to 20 and 50 ppm in solution at 25 °C. The oxidative degradation of caffeine was carried out using a fresh catalyst for each test. Liquid samples were taken after 1 h of dark adsorption, and 1, 3, 7 and 22 h after  $\text{H}_2\text{O}_2$  was added. The concentration of caffeine in the solution was determined by measuring the absorbance of the filtered solution at 484 nm on an Evolution 220 UV–Vis spectrophotometer (Thermo Fisher Sci.). Experimental variation for the concentration of caffeine in the solution was  $\pm 0.8$  ppm. Total organic carbon (TOC) analysis was undertaken on a Shimadzu TOC analyzer with an Agilent Eclipse XDB-C8  $4.6 \times 150$  mm column with  $5\text{ }\mu\text{m}$  packing. The TOC analysis was carried out on a 150  $\mu\text{L}$  sample, and

the organic carbon content was an average value calculated from four measurements for each tested catalyst and tested condition.

### 3. Results and discussion

The incorporation of Fe in MFI zeolites was carried out during zeolite formation, by a two-steps microwave-assisted hydrothermal synthesis method. Fe-MFI was produced from solutions with Si/Fe atomic ratios equal to  $\infty$  (0 %Fe), 400 (0.25 %Fe), 200 (0.5 %Fe), 100 (1 %Fe) and 50 (2 %Fe), though the 25 (4%Fe) samples failed due to direct gelation of the sol. The Fe concentration in the produced powders, determined by EDS, generally showed a good transfer of Fe ions from the sol (0.25, 0.5, 1 and 2%) to the synthesized bulk materials resulting in measured Fe concentrations of 0.34, 0.66, 1.20 and 2.33 % in the solids, respectively. A wide angle XRD analysis was also conducted as displayed in Fig. 1 in order to determine the crystal structure of the materials. The measured patterns were compared to the reported in a PDF2 data basis and were attributed to reference pattern 01-070-4744. These XRD patterns confirm that all formed materials hold the monoclinic crystal structure (#14, P21/n1), characteristic for calcined MFI structure.

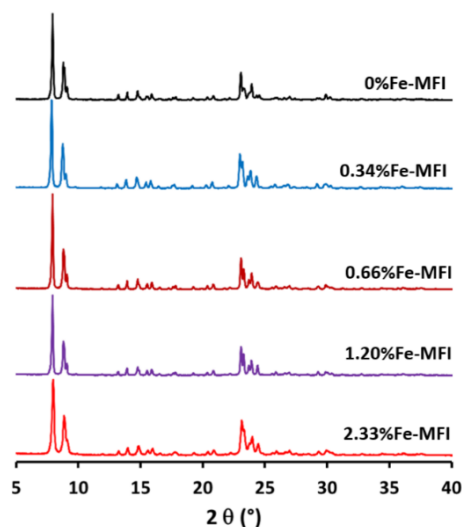




Fig. 1 XRD patterns of pure MFI (silicalite-1) and Fe-MFI powders (FeS-1) series calcined at 550 °C.

Table 1 lists the lattice parameters (a, b, and c) calculated from XRD patterns. As expected for an isomorphous substitution of Si by Fe, the unit cell volume increased when 0.25% Fe was incorporated into the synthesis solution as compared with the blank 0%Fe-MFI sample. However, the cell volume values did not correlate with the quantity of Fe detected by EDS. Rather, the unit cell volume peaked as x increased from 0 to 0.34%, before decreasing sequentially for higher Fe content. The  $\beta$  parameter, which is related to the crystal lattice distortion, evolved by a different profile to the unit cell volume, peaking at Fe concentration of 1.20%. Interestingly, no secondary iron oxide phase was detected in the XRD patterns, thus confirming the presence of monoclinic crystal structure (#14, P21/n1) (Treacy and Higgins, 2001). It is noteworthy that Fe-MFI zeolites were synthesized with Fe concentration in excess of 1% (i.e. Si/Fe < 100).

Table 1. Fe concentration in both sols and derived solids, and lattice constants of the corresponding MFI zeolites. x was measured by EDS. (atom %)

x%Fe-MFI sample						
sol	0	0.25	0.50	1.00	2.00	
solid (x)	0	0.34	0.66	1.20	2.33	
a (Å)	20.056 (5)	20.030 (4)	20.250 (1)	20.110 (3)	19.970 (1)	
b (Å)	19.990 (5)	20.069 (5)	20.158 (8)	20.140 (3)	20.100 (1)	
c (Å)	13.401 (3)	13.396 (4)	11.197 (5)	11.140 (2)	11.045 (8)	
$\alpha, \beta$ (°)	90, 90	90, 90	90, 90	90, 90	90, 90	

$\gamma$ (°)	89.922 (3)	90.124 (4)	90.266 (7)	90.900 (3)	90.420 (1)
Vol. (Å <sup>3</sup> )	5373	5385	4571	4511	4433

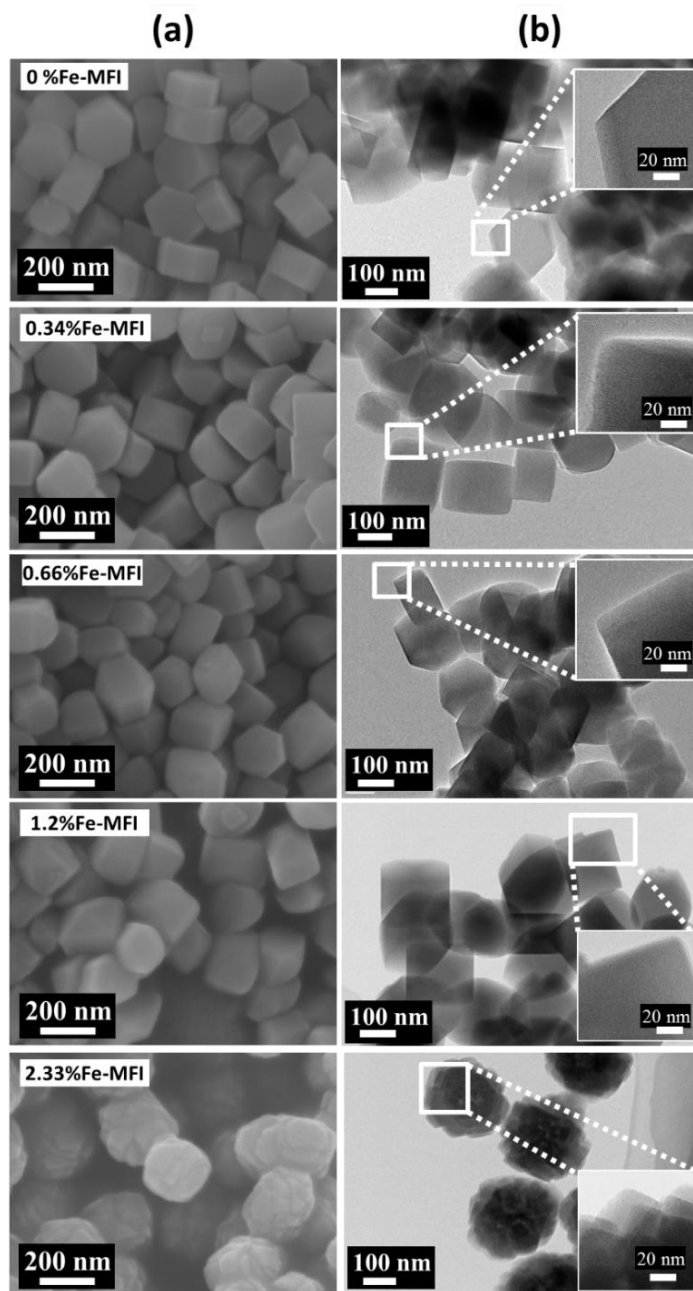


Fig. 2 (a) SEM and (b) TEM with HR-TEM inset images of pure MFI (S-1) and Fe-MFI (FeS-1) powders series.

The FE-SEM images in Fig. 2a clearly show that the MFI zeolite morphology was influenced by the Fe concentration. For instance, by raising the Fe concentration from 0 to 1.20%, the particles were getting rounder every time the Fe concentration was increased. Further increase of x from 1.20% Fe to 2.33% Fe yielded a packed and aggregated structure, resembling a cauliflower, comprised of smaller cubic crystals (< 100 nm). TEM images in Fig. 2b confirmed the formation of single crystal particles in samples derived from sols with the lowest iron concentrations (0 to 1.20% Fe). They are common features of MFI type zeolite morphology. Further increase of the Fe content at 2.33% resulted in a more complex polycrystalline structure made of aggregated cubic nanocrystals 40 nm in size.

To shed further light on Fe-MFI formation, Raman spectroscopy analysis was carried out to understand the incorporation of Fe ions. Fig. 3 shows two bands common to all samples (with and without Fe) at  $378\text{ cm}^{-1}$ . The band at  $378\text{ cm}^{-1}$  is associated to with the Si–O–Si vibrations. The bands at  $1165$ ,  $1019$  and  $516\text{ cm}^{-1}$  were common to the iron-containing samples only. The bands at  $1165$  and  $1019\text{ cm}^{-1}$  were assigned to vibrational bands of Si–O–Si near iron and Fe–O–Si, respectively, and the  $516\text{ cm}^{-1}$  band was assigned to  $\text{Fe}(\text{O})_4$  in the zeolite network (Fan et al., 2009). Any additional bands potentially allocated to iron oxide particles (li et al., 2012) could not be observed at given conditions. Coupled with the absence of nano-particle domains in the HR-TEM images in Fig. 2b, these results clearly indicate that Fe was mainly incorporated in MFI particles as intra-framework species rather than as iron oxide (i.e. extra-framework) particles.

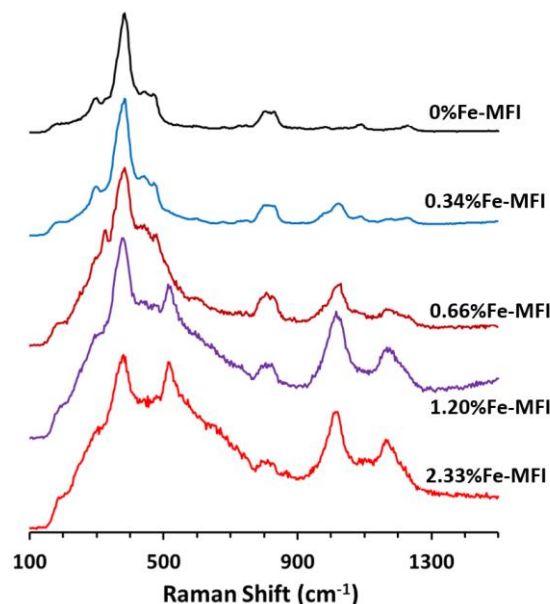


Fig. 3 Raman spectra of pure MFI and Fe-MFI samples.

A further insight into the microstructure of the synthesized zeolites is displayed by their pore size distribution (PSD) (Fig. 4a) determined by the density functional theory (DFT) from N<sub>2</sub> sorption isotherms (Fig. 4b). The incorporation of Fe into MFI conferred both mesoporosity and microporosity to the powders, contrary to the microporosity of pure MFI. This can be further verified by the shift in the average PSD from 10 Å of pores not related to zeolite framework for the pure 0%Fe-MFI to 22, 27 and 30 Å for the 2.33%, 1.20% and 0.66%Fe-MFI samples, respectively. Although microporous features were maintained with the incorporation of Fe, the isotherms of the Fe-MFI powders clearly indicates the formation of large micropores and finally mesopores for the higher Fe concentrations. The BET surface areas increased by Fe incorporation from 336 (0%Fe-MFI) to 414 (0.34%Fe-MFI), 415 (0.66%Fe-MFI), 386 (1.2%Fe-MFI) and 396 m<sup>2</sup> g<sup>-1</sup> (2.33%Fe-MFI), which were in the range of literature data for MFI zeolites (Jung et al., 2009 and Li et al., 2013).

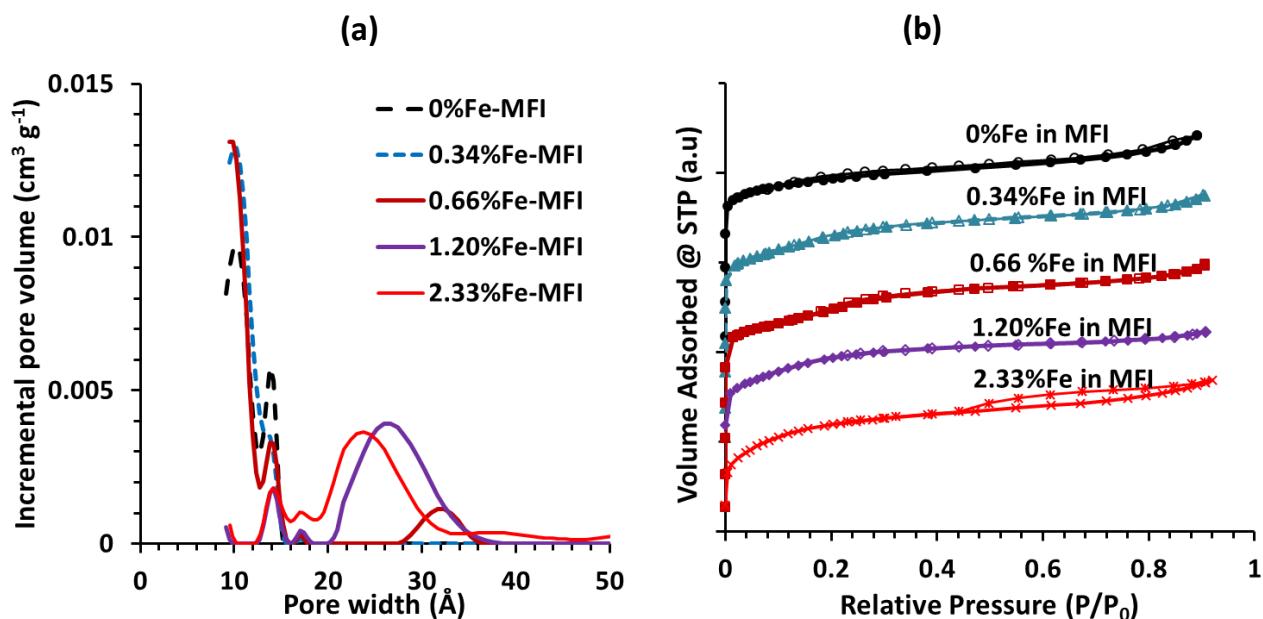


Fig. 4 (a) Pore size distribution and (b) nitrogen sorption isotherms of Fe-MFI and MFI samples.

The as-synthesized Fe-MFI samples were used as catalysts in a Fenton-like heterogeneous reaction as described in the experimental section. Fig. 5a clearly shows that the blank sample (%Fe-MFI) was unable to breakdown caffeine within 7 hours reaction, and only minor degradation was observed by 22 hours. Similar trends were also observed for the 0.34% and 0.66%Fe-MFI samples, which gave very low caffeine degradation rates. However, the results in Fig. 5a strongly suggest that the Fe has to be above a certain concentration to be effective in catalysis, in this case at least 1.20% Fe within the MFI powder. For comparison purpose, a commercially available Fenton like catalyst  $\text{Fe}_3\text{O}_4$  was also tested for the degradation of caffeine reaching. The results in Fig 5a confirm that the Fe-MFI zeolite catalysts were more efficient than the  $\text{Fe}_3\text{O}_4$  catalyst. For instance, caffeine degradation of up to 98% and 90% were achieved by the 2.33%

and 1.23% Fe-MFI at 20 h, respectively, whilst the  $\text{Fe}_3\text{O}_4$  catalyst reached a maximum degradation of 82%.

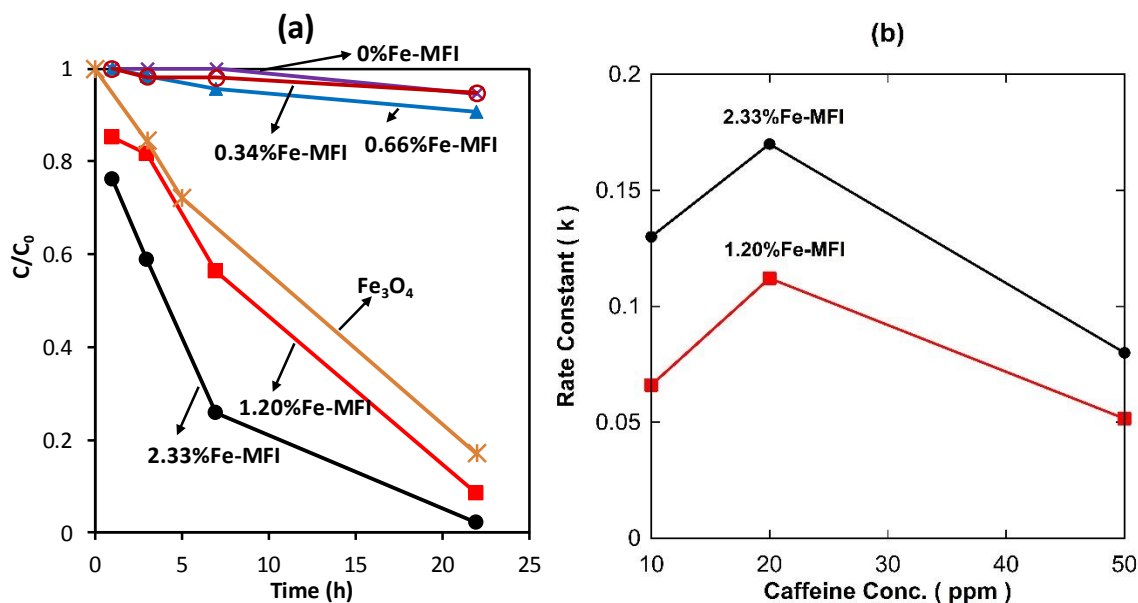


Fig. 5 (a) Caffeine degradation at concentration of 10 ppm in aqueous solution, and (b) rate constant at 10, 20 and 50 ppm @ 7 hours. All experimental conditions:  $\text{H}_2\text{O}_2=22$  mM, pH=3 and 25 °C.

Fig. 5b displays the rate constant ( $k$ ) for the same experimental work by varying the initial concentration of caffeine from 10 to 50 ppm for the most active samples (2.33% and 1.20% Fe-MFI). Again these results demonstrate that the  $k$  values were greater for higher Fe content in the zeolite structure (2.33% Fe-MFI). The  $k$  value consistently increased from 10 to 20 ppm, and then reduced when caffeine concentration increased further to 50 ppm. The reduction of the  $k$  value is associated with mass transfer limitations as adsorption was found to be negligible (~1%). Further, as the surface area of the Fe containing MFI samples were very similar, the higher  $k$  values of 2.33% Fe-MFI were therefore related to the amount of incorporated Fe.

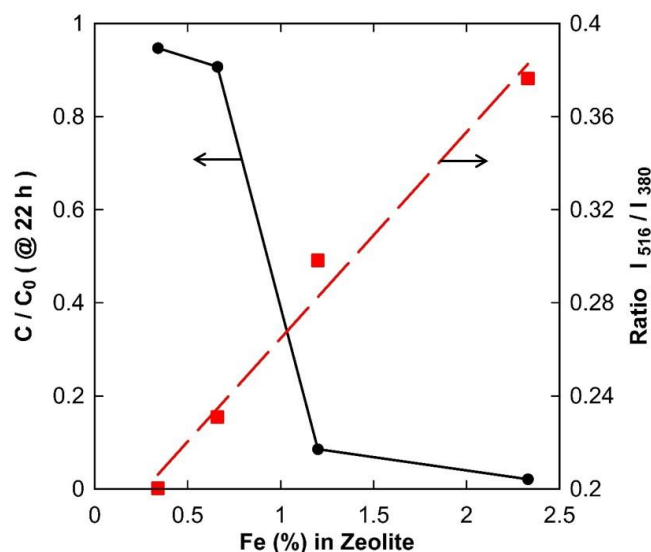
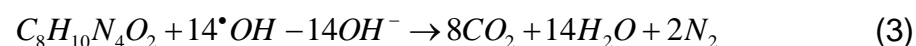
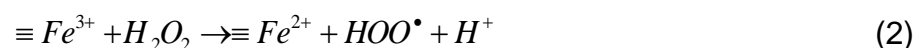


Fig. 6 Caffeine degradation and ratio of Raman peak areas at 516 and 378  $\text{cm}^{-1}$  as the function of iron fraction in Fe-MFI zeolite powders.

In order to explain the improved performance of Fe-MFI samples, the Raman spectra in Fig. 3 were deconvoluted to calculate the ratio of peak areas assigned to vibrational bands of the intra-framework species containing iron oxygen bonds ( $\text{Fe}(\text{O})_4$ ) at 516  $\text{cm}^{-1}$  over the MFI building units band at 378  $\text{cm}^{-1}$ . Fig. 6 shows that the  $I_{516}/I_{378}$  ratio increased almost linearly with an increase of iron content, showing good  $R^2$  fitting correlations (0.982). This fitting confirmed the linearity within the Fe-MFI range in this work and the validity of the Raman deconvolution proposed by Fan and co-workers (Fan et al., 2010). In conjunction with the catalyst activity in Fig. 4a, the results in Fig. 6 strongly suggest that there is significant correlation between the presence of  $\text{Fe}(\text{O})_4$  sites and enhanced degradation of caffeine for Fe concentrations higher than 1.20% in the zeolite. The  $\text{Fe}(\text{O})_4$  sites are thus active in a Fenton-like process. This was accompanied by the presence of mesopores ( $20 < d < 35 \text{ \AA}$ ) in the 1.20% and 2.33% Fe-MFI samples which favored the

diffusion of the small caffeine molecules (length: 10 Å) (Banerjee et al., 2012) into the zeolite structure. The very low catalytic activity of the other Fe-MFI samples was attributed to both insufficient Fe concentration, below 1.20% Fe, and microporosity leading to mass transfer limitations.

Due to the large surface areas of the Fe-MFI powders (~380–390 m<sup>2</sup> g<sup>-1</sup>), solid-liquid interface reactions occurred preferentially at the Fe(O)<sub>4</sub> sites. This reaction is schematically shown in Fig. 8 as isomorphic Fe(O)<sub>4</sub> sites embedded into the zeolite structure degrade caffeine. In this reaction, H<sub>2</sub>O<sub>2</sub> was catalytically decomposed at the Fe<sup>2+</sup> active sites into <sup>•</sup>OH radicals and OH<sup>-</sup> hydroxyl ions (Eq. 1). As proposed by Gonzalez-Olmos and co-workers (Gonzalez-Olmos, 2011), Fe<sup>2+</sup> active sites are generated by the reaction of H<sub>2</sub>O<sub>2</sub> with isolated Fe<sup>3+</sup> sites at the Fe-MFI surface or by <sup>•</sup>OOH radicals formed previously in the reaction of H<sub>2</sub>O<sub>2</sub> with Fe<sup>3+</sup> (Eq. 2). As confirmed by TOC analysis (Fig. 7), the powerful <sup>•</sup>OH radicals mineralized the caffeine (C<sub>8</sub>H<sub>10</sub>N<sub>4</sub>O<sub>2</sub>) into CO<sub>2</sub>, H<sub>2</sub>O and N<sub>2</sub> species (Eq. 3). TOC analysis also confirms the degradation ratio ascertained by UV-vis measurement (Fig. 6), showing very high level of mineralization of caffeine at 94.5 and 96.0% for the 1.20% and 2.33% Fe-MFI samples, respectively. Therefore, this reaction is characterized by the reduction of Fe<sup>3+</sup> to Fe<sup>2+</sup> and oxidation of Fe<sup>2+</sup> to Fe<sup>3+</sup>, concomitantly with the mineralization of caffeine. Provided H<sub>2</sub>O<sub>2</sub> is supplied, these results demonstrate the potential of Fe-MFI zeolites to treat waters contaminated with caffeine micro-pollutants.





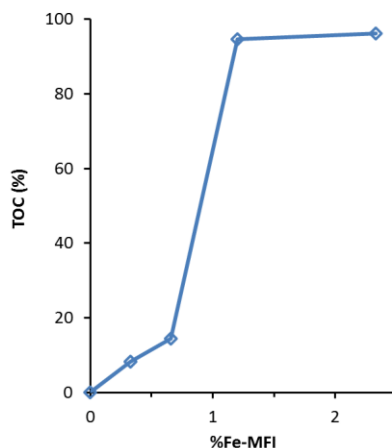


Fig. 7 TOC values of 10 ppm caffeine solution after 22h using Fe-MFI zeolites with varying Fe content.

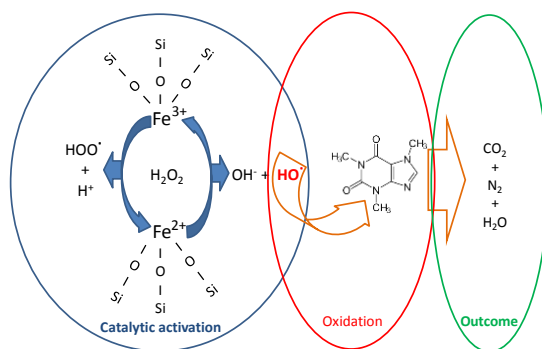


Fig. 8 Schematic representation of the reaction mechanism using Fe-MFI zeolite in the heterogeneous Fenton-like reaction for caffeine degradation in this work.

The best performing 2.33%Fe-MFI catalyst was also tested for multiple reaction cycles and compared against the commercial  $\text{Fe}_3\text{O}_4$ . Fig. 9a shows that the 2.33%Fe-MFI catalyst maintained a constant caffeine degradation efficiency of 98% up to the tested 5 cycles. Contrary to this, the commercial  $\text{Fe}_3\text{O}_4$  catalyst degradation declined very quickly after the first cycle, and at the fourth cycle this catalyst was unable to degrade caffeine. This fast decrease in degradation efficiency is associated with the oxidation of the active

phase  $\text{Fe}^{2+}$  into a non-active phase  $\text{Fe}^{3+}$  in  $\text{Fe}_3\text{O}_4$  based catalysts (Zubir et al., 2015). In the case of the Fe-MFI catalyst, the multiple cycling stability strongly suggests that the active phase was maintained. This is confirmed by the Raman analysis (Fig.9b) which shows that the spectrum of the fresh sample remained unaltered after 5 cycles of caffeine degradation, thus confirming the catalytic stability of Fe-MFI upon cycling.

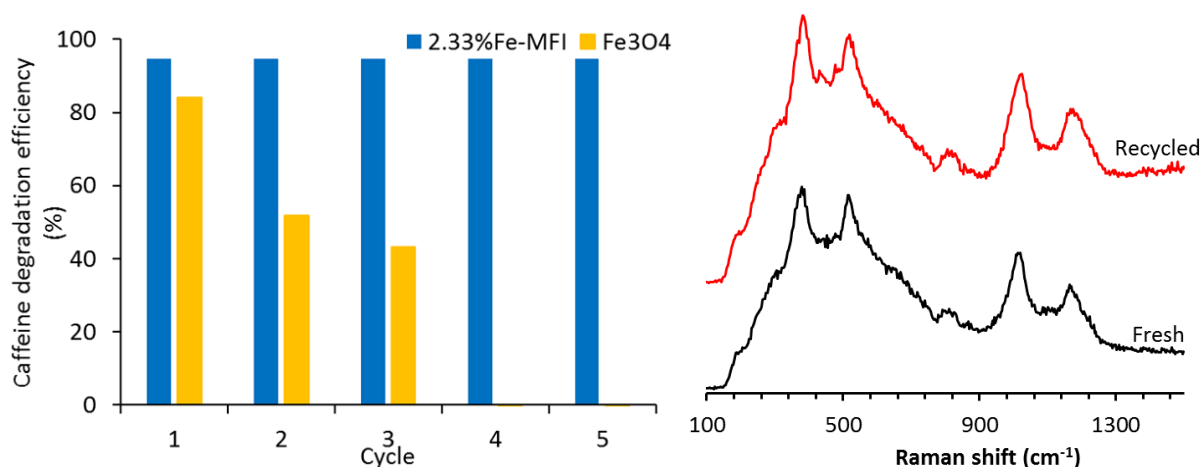


Fig. 9 (a) Cycling experiment conducted on 2.33%Fe-MFI zeolites and commercial  $\text{Fe}_3\text{O}_4$  in a caffeine degradation ( $C_{\text{caffeine}} = 10 \text{ ppm}$ ) at 20 h per cycle; (b) Raman spectra of fresh and a sample 2.33%Fe-MFI zeolite exposed to 5 cycles of caffeine degradation.

#### 4. Conclusions

The incorporation of Fe with concentrations above 1.0% conferred mesoporosity to the Fe-MFI, thus facilitating the access of caffeine to the zeolite porous structure. The  $\text{Fe}(\text{O})_4$  bonds in the Fe-MFI zeolite structure were very active leading to the decomposition of  $\text{H}_2\text{O}_2$  into radicals, thus promoting the degradation of caffeine in the heterogeneous Fenton-like reaction. The significant increase in catalytic activity was attributed to

mesoporosity coupled with Fe concentrations at and above 1.20% in the MFI structure.

TOC removal of 96% with 2.33%Fe-MFI sample was achieved.

## Acknowledgment

The authors acknowledge the facilities, and the scientific and technical assistance, of the Australian Microscopy & Microanalysis Research Facility at the Centre for Microscopy and Microanalysis, The University of Queensland. A. Julbe and J.C. Diniz da Costa would like to acknowledge the financial support for international collaboration from the Centre National de la Recherche Scientifique (CNRS-INC) in France. J. C. Diniz da Costa acknowledges support given by the Australian Research Council (ARC) Future Fellowship program (FT130100405).

## References

Anizelli P.R., Baú, J.P.T., Valezi, D.F., Canton, L.C., Carneiro, C.E.A., Di Mauro, E., da Costa, A.C.S., Galante, D., Braga, A.H., Rodrigues, F., Coronas, J., Casado-Coterillo, C., Zaia, C.T.B.V., Zaia D.A.M., 2016. Adenine Interaction with and Adsorption on Fe-ZSM-5 zeolites: a Prebiotic Chemistry Study Using Different Techniques, *Micro. Meso. Mat.* 226, 493-504.

An, W., Xiao, X., Yu, M., Chen, X., Xu, Y., Zhou, W., 2013. Adsorptive Removal of Trace Oxytetracycline from Water by Acid-Modified Zeolite: Influencing Factors. *Water Sci. Technol.* 68, 2473-2478.

- 1  
2  
3  
4 Banerjee, S., Verma, P., Mitra, R., Basu, G., Pal, S., 2012. Probing the Interior of Self-  
5 assembled Caffeine Dimer at Various Temperatures. *J. Fluoresc.* 22, 753-769.  
6  
7  
8  
9 Bordiga, S., Buzzoni, R., Geobaldo, F., Lamberti, C. Giamello, E., Zecchina, A.,  
10 Leofanti, G., Petrini, G., Tozzola, G., Vlaic, G., 1996. Structure and reactivity of  
11 framework and extraframework iron in Fe-silicalite as investigated by spectroscopic  
12 and physicochemical methods, *J. Catal.* 158 (2), 486–501.  
13  
14  
15  
16  
17  
18 Bruton, T., Alboloushi, A., de la Garza, B., Kim, B.O., Halden, R.U., 2010. Fate of  
19 Caffeine in the Environment and Ecotoxicological Considerations. *J. Am. Chem.*  
20 *Soc.* 1048, 257-273.  
21  
22  
23  
24  
25  
26 Buerge, I.J., Poiger, T., Müller, M.D., Buser, H.-R., 2003. Caffeine, an Anthropogenic  
27 Marker for Wastewater Contamination of Surface Waters. *Env. Sci. Technol.* 37,  
28 691-700.  
29  
30  
31  
32  
33 Christensen, C.H., Johannsen, K., Schmidt, I., Christensen, C.H., 2003. Catalytic  
34 Benzene Alkylation over Mesoporous Zeolite Single Crystals: Improving Activity  
35 and Selectivity with a New Family of Porous Materials. *J. Am. Chem. Soc.* 125 (44),  
36 13370–13371.  
37  
38  
39  
40  
41  
42  
43 Fan, F., Feng, Z., Li, C., 2010. UV Raman Spectroscopic Study on the Synthesis  
44 Mechanism and Assembly of Molecular Sieves. *Chem. Soc. Rev.* 39, 4794-4801.  
45  
46  
47  
48 Fan, F., Sun, K., Feng, Z., Xia, H., Han, B., Lian, Y., Ying, P., Li, C., 2009. From  
49 Molecular Fragments to Crystals: a UV Raman Spectroscopic Study on the  
50 Mechanism of Fe-ZSM-5 Synthesis. *Chem. – A Eur. J.* 15, 3268-3276.  
51  
52  
53  
54  
55 Franzoso, F., Nisticò, R., Cesano, F., Corazzari, I., Turci, F., Scarano, D., Prevot, A.B.,  
56 Magnacca, G., Carlos, L., Mártire, D.O., 2017. Biowaste-derived substances as a  
57  
58  
59  
60  
61  
62  
63  
64  
65

1  
2  
3  
4 tool for obtaining magnet-sensitive materials for environmental applications in  
5  
6  
7 wastewater treatments Chem. Eng. J. 310, 307–316.  
8  
9 Gao, Y., Wang, Y., Zhang, H., 2015. Removal of Rhodamine B with Fe-supported  
10  
11 Bentonite as Heterogeneous Photo-Fenton Catalyst under Visible irradiation. Appl.  
12  
13 Cat. B: Env. 178, 29-36.  
14  
15  
16 Giordano, G., Katovic, A., Perathoner S., Pino, F. Centi, G. Nagy, J.B., Lazar, K., Fejes,  
17  
18 P, 2002. One-step benzene oxidation to phenol—part I: preparation and  
19  
20 characterization of Fe-(Al)MFI type catalysts, Stud. Surf. Sci. Catal., 142, 477–484.  
21  
22  
23 Gonzalez-Olmos, R., Holzer, F., Kopinke, F.-D., Georgi A., 2011. Indications of the  
24  
25 Reactive Species in a Heterogeneous Fenton-Like Reaction Using Fe-Containing  
26  
27 Zeolites. App. Catal. A: General. 398, 44-53.  
28  
29  
30  
31 Gummadi, S.N., Ganesh, K.B., Santhosh, D., 2009. Enhanced Degradation of Caffeine  
32  
33 by Immobilized Cells of Pseudomonas sp. in Agar-Agar Matrix Using Statistical  
34  
35 Approach. Biochem. Eng. J. 44, 136-141.  
36  
37  
38 Hoffmann, K., Marlow, F., Caro, J., 1997. Photoinduced Switching in Nanocomposites  
39  
40 of Azobenzene and Molecular Sieves. Adv. Mater. 9 (7) 567-570.  
41  
42  
43 Jung, J., Jo, C., Mota, F.M., Cho, J., Ryoo R., 2015. Acid Catalytic Function of  
44  
45 Mesopore Walls Generated by MFI Zeolite Desilication in Comparison with  
46  
47 External Surfaces of MFI Zeolite Nanosheet. Appl. Catal. A Gen. 492, 68-75.  
48  
49  
50  
51 Klammerth, N., Malato, S., Agüera, A., Fernández-Alba, A., Mailhot, G., 2012. Treatment  
52  
53 of Municipal Wastewater Treatment Plant Effluents with Modified Photo-Fenton as  
54  
55 a Tertiary Treatment for the Degradation of Micro Pollutants and Disinfection.  
56  
57 Environ. Sci. Technol. 46, 2885–289.  
58  
59  
60  
61  
62  
63  
64  
65

- 1  
2  
3  
4 Kragović, M., Daković, A., Marković, M., Krstić, J., Gatta, G.D., Rotiroti, N., 2013.  
5  
6 Characterization of Lead Sorption by the Natural and Fe (III)-modified Zeolite. Appl.  
7  
8 Surf. Sci. 283, 764-774.  
9
- 10  
11 Kritchayanon, N., Thanabodeekij, N., Jitkarnka, S., Jamieson, A.M., Wongkasemjit, S.,  
12  
13 2006. Synthesis, of Fe-loaded MFI Zeolite Using Silatrane as Precursor and its CO  
14  
15 Activity. Appl. Organometallic Chem. 20, 155-160.  
16  
17
- 18  
19 Li, J.P.H., Kennedy, E., Stockenhuber, M., 2014. Oxidative Coupling and Hydroxylation  
20  
21 of Phenol over Transition Metal and Acidic Zeolites: Insights into Catalyst Function.  
22  
23 Catal. Lett. 144, 9–15.  
24  
25
- 26  
27 Li, X., Li, B., Xu, J., 2013. Synthesis and Characterization of Transitional Metal-rich  
28  
29 Zeolite M-MFI (M=Fe, Co, Ni, Cu) with Regular Mesoporous Channels. Coll. Surf.  
30  
31 A Physicochem. Eng. Asp. 434, 287-295.  
32  
33
- 34  
35 Li, Y.-S., Church, J.S., Woodhead, A.L., 2012. Infrared and Raman Spectroscopic  
36  
37 Studies on Iron Oxide Magnetic Nano-particles and their Surface Modifications. J.  
38  
39 Magnetism Magnetic Mater. 324, 1543-1550.  
40
- 41  
42 Liu, C., Li, J., Qi, J., Wang, J., Luo, R., Shen, J., Sun, X., Han, W., Wang, L., 2014.  
43  
44 Yolk-shell Fe(0)@SiO<sub>2</sub> Nanoparticles as Nanoreactors for Fenton-like Catalytic  
45  
46 Reaction. ACS Appl. Mater. Interfaces 6, 13167–13173.  
47
- 48  
49 Maxwell, I.E., van den Brink, P., Downing, R.S., Sijpkens, A.H., Gomez S., Maschmeyer,  
50  
51 T., 2004. High-throughput Technologies to Enhance Innovation in Catalysis. Top.  
52  
53 Catal. 24, 125-135.  
54
- 55  
56 Meng, Q., Doetschman, D.C., Rizos, A.K., Lee, M.-H., Schulte, J.T., Spyros, A., Kanyi,  
57  
58 C.W., 2011. Adsorption of Organophosphates into Microporous and Mesoporous  
59  
60  
61  
62  
63  
64  
65

- NaX Zeolites and Subsequent Chemistry, *Environ. Sci. Technol.* 45 (7), 3000–3005.
- Mijangos, F., Varona, F., Villota, N., 2006. Changes in Solution Color During Phenol Oxidation by Fenton Reagent. *Environ. Sci. Technol.*, 40, 5538–5543
- Moliner, M., 2012. Direct Synthesis of Functional Zeolitic Materials, *ISRN Materials Science*, (2012), <http://dx.doi.org/10.5402/2012/789525>.
- Pérez-Ramírez, J., Christensen, C.H., Egeblad, K., Christensen, C. H., Groen J. C., 2008. Hierarchical zeolites: enhanced utilisation of microporous crystals in catalysis by advances in materials design, *Chem. Soc. Reviews* 37 (11), 2530–2542.
- Rangnekar, N., Mittal, N., Elyassi, B., Caro, J., Tsapatsis, M., 2015. Zeolite membranes - a review and comparison with MOFs, *Chemical Society Reviews* 44 (20), 7128-7154.
- Rodriguez del Rey, Z., Granek E.F., Sylvester, S., 2012. Occurrence and Concentration of Caffeine in Oregon Coastal Waters. *Marine Poll. Bull.* 64, 1417-1424.
- Rodríguez, S., Santos, A., Romero, A., 2017. Oxidation and priority and emerging pollutants with persulfate activated by iron: Effect of iron valence and particle size, *Chem. Eng. J.* 318, 197-205.
- Rosal, R., Rodríguez, A., Perdigón-Melón, J.A., Petre, A., García-Calvo, E., Gómez, M.J., Agüera, A., Fernández-Alba, A.R., 2009. Degradation of Caffeine and Identification of the Transformation Products Generated by Ozonation. *Chemosphere* 74, 825-831.

- Taniguchi, T., Nakasaka, Y., Yoneta, K., Tago, T., Masuda, T., 2016. Size-controlled synthesis of MFI metallosilicate and their catalytic performance on acetone to olefins reaction, *Micro. Meso. Mat.* 224, 68-74.
- Treacy, M. M. J., Higgins, J. B., 2001. Collection of Simulated XRD Powder Patterns for Zeolites, fourth ed., Elsevier, Amsterdam.
- Vermeiren W., Gilson, J.P., 2009. Impact of zeolites on the petroleum and petrochemical industry, *Topics in Catalysis* 52 (9), 1131–1161.
- Wang, Y., Zhao, G., Chai, S., Zhao, H., Wang, Y., 2013. Three-dimensional Homogeneous Ferrite-Carbon Aerogel: One Pot Fabrication and Enhanced Electro-Fenton Reactivity. *ACS Appl. Mater. Interfaces* 5, 842–852.
- Wingenfelder, U., Hansen, C., Furrer, G., Schulin, R., 2005. Removal of Heavy Metals from Mine Waters by Natural Zeolites, *Environ. Sci. Technol.* 39 (12), 4606–4613.
- Zeng, T., Zhang, X., Wang, S., Niu, H., and Cai. Y., 2015. Spatial Confinement of a  $\text{Co}_3\text{O}_4$  Catalyst in Hollow Metal–Organic Frameworks as a Nanoreactor for Improved Degradation of Organic Pollutants. *Environ. Sci. Technol.* 49 (4), 2350-2357
- Zubir, N.A., Yacou, C., Motuzas, J., Zhang, X., Diniz da Costa, J.C., 2014. Structural and Functional Investigation of Graphene Oxide- $\text{Fe}_3\text{O}_4$  Nanocomposites for the Heterogeneous Fenton-like Reaction. *Sci. Rep.* 4, 4594, DOI: 10.1038/srep04594.
- Zubir, N.A., Yacou, C., Motuzas, J., Zhang, X., Zhao, X.S., Diniz da Costa, J.C., 2015. The Sacrificial Role of Graphene Oxide in Stabilising a Fenton-like Catalyst  $\text{GO}-\text{Fe}_3\text{O}_4$ . *Chem. Commun.* 51, 9291-9293.